RESEARCH ADVANCE

Figures and figure supplements

Parallel processing, hierarchical transformations, and sensorimotor associations along the 'where' pathway

Raymond Doudlah *et al*

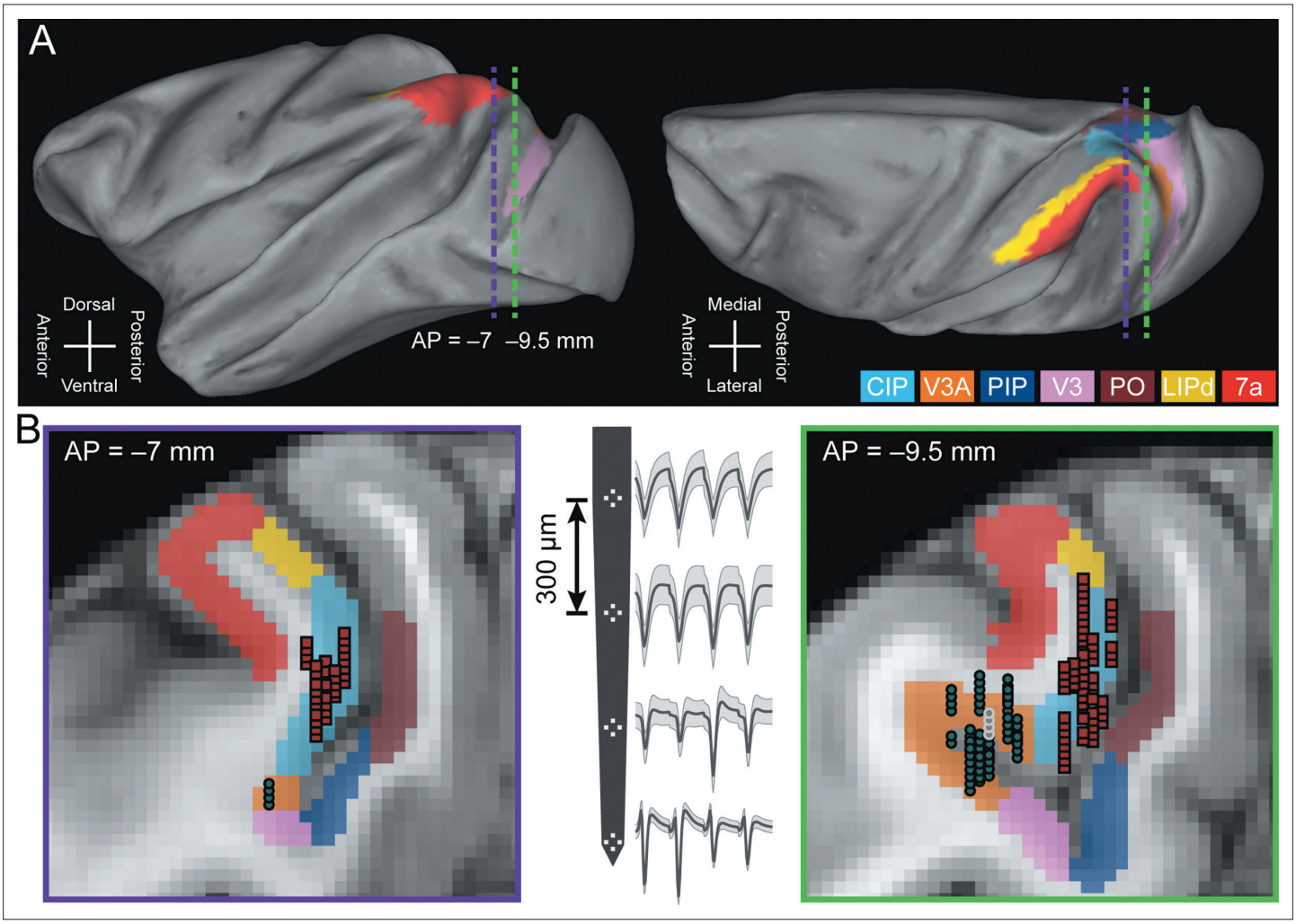

Figure 1. Neuronal recordings. (**A**) Lateral (left) and dorsal (right) views of the inflated cortical surface of Monkey L (left hemisphere). Dashed lines mark the coronal sections in (**B**). (**B**) Coronal sections (left: AP = –7 mm; right: AP = –9.5 mm) with MRI-based estimates of the boundaries of V3A, CIP, and adjacent areas. Recording locations for V3A (blue-gray circles) and CIP (red squares) were projected along the AP axis onto the closest of the two coronal sections shown. A schematic of a four-tetrode laminar probe with spike waveforms from the V3A recording marked with white circles in the right coronal section is shown (middle). CIP, caudal intraparietal area (light blue); V3A, visual area V3A (orange); PIP, posterior intraparietal area; V3, visual area V3; PO, parieto-occipital area; LIPd, dorsal aspect of the lateral intraparietal area; 7a, area 7a.

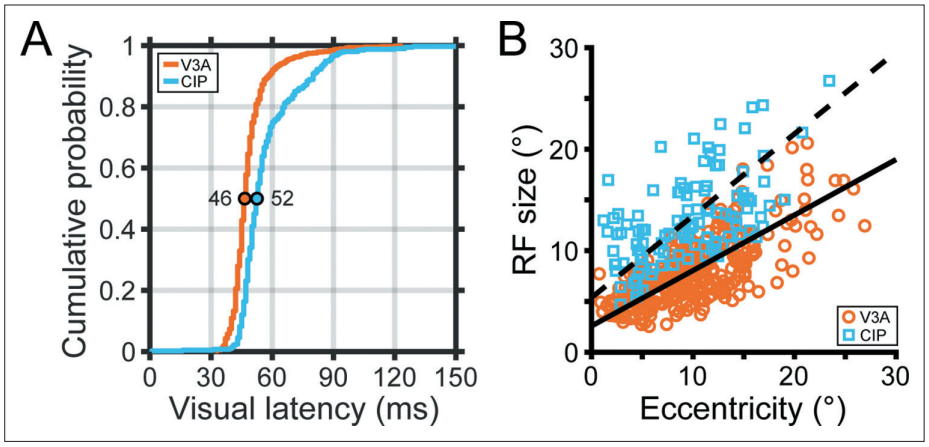

Figure 1—figure supplement 1. Response latencies and receptive field sizes. (**A**) Cumulative density functions for the visual latencies of visual area V3A (V3A) (orange) and caudal intraparietal (CIP) area (blue) neurons. Colored circles mark the median latencies. (**B**) Receptive field (RF) size versus eccentricity for V3A (orange circles) and CIP (blue squares). RF size was defined as the square root of the RF area. Type II regression lines are shown for V3A (solid line; RF size = 2.6 + 0.55 × eccentricity) and CIP (dashed line; RF size = 5.4 + 0.81 × eccentricity).

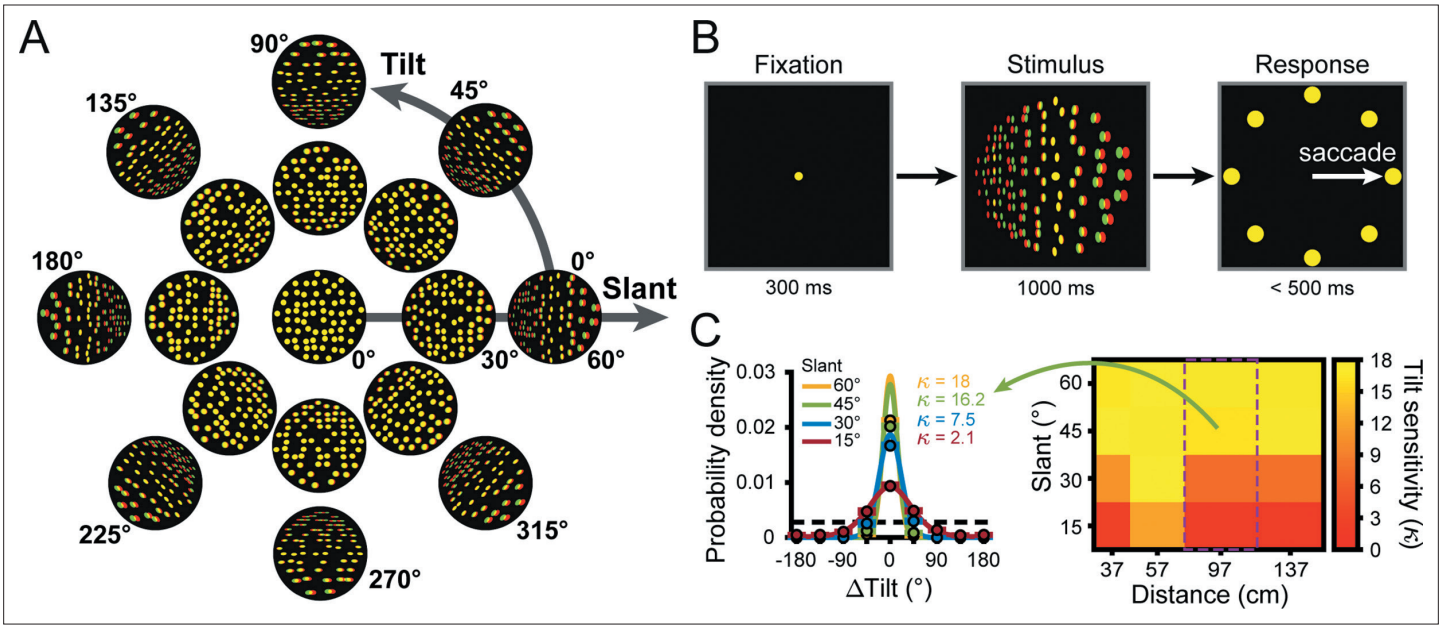

Figure 2. Stimuli, task, and behavioral performance. (**A**) Planar surfaces were defined using random dots with perspective and stereoscopic cues (illustrated here as red-green anaglyphs). For clarity, the size and number of dots differ from the actual stimuli. (**B**) Eight-alternative tilt discrimination task. A trial began by fixating a dot at the center of the screen (fixation was always at screen distance, 57 cm) for 300 ms (left). A plane was then presented with a given tilt (0–315°, 45° steps), slant (0–60°, 15° steps), and distance (37, 57, 97, or 137 cm) for 1 s (middle). The fixation target and plane then disappeared and eight choice targets corresponding to the eight tilts appeared (right). This cued the monkey to saccade to one of the targets to report which side of the plane was nearest. (**C**) Behavioral performance. Error distributions of reported tilts for each slant at 97 cm for Monkey W (left). Data points show the mean probability of a given ΔTilt (reported tilt – presented tilt), and error bars show standard error of the mean (SEM) across sessions (N = 14). Solid curves are von Mises probability density functions with sensitivities (κ) indicated. The black dashed line marks chance level. The heat map (right) shows the mean tilt sensitivity for each slant (rows) and distance (columns) for Monkey W across sessions. Yellow hues indicate higher sensitivities. Green arrow and purple rectangle mark the data shown in the error distribution plots (left).

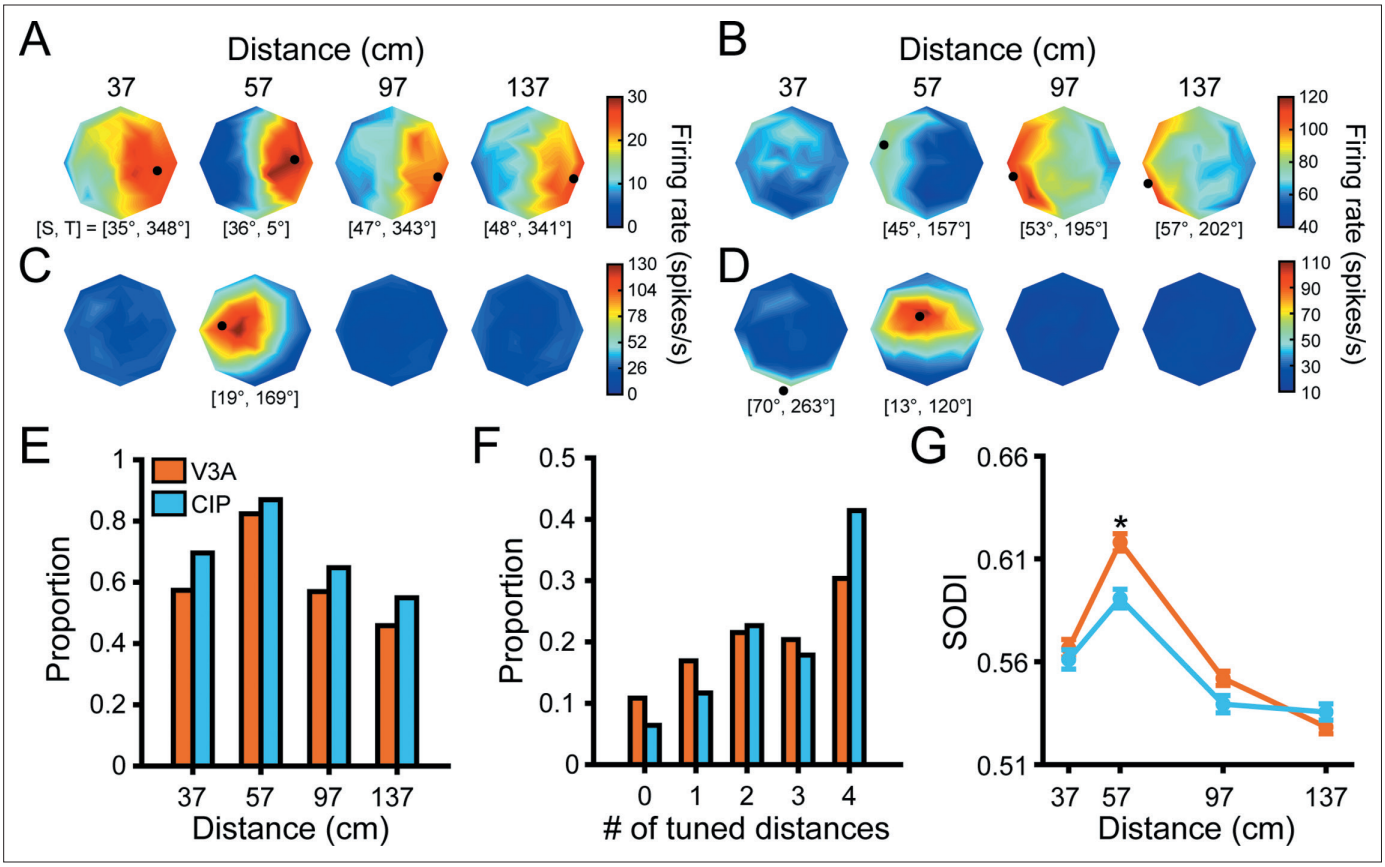

Figure 3. Comparison of 3D orientation tuning across distance. (**A–D**) Four example visual area V3A (V3A) neurons from Monkey W (**A, C**) and Monkey F (**B, D**). Heat maps show firing rate plotted as a function of tilt (angular axis) and slant (radial axis). Red hues indicate higher firing rates. Black dots mark preferred 3D orientations from Bingham function fits at distances with significant tuning (ANOVA, $p<0.05$; Bonferroni–Holm corrected for four distances). Some dots are not located on a disc because the largest tested slant was 60° but slant ranges from 0° to 90°. The preferred slant (S) and tilt (T) are indicated for each tuned distance. (**E**) Proportion of neurons with significant orientation tuning at each distance for V3A (orange; proportions: 37 cm = 0.57, 57 cm = 0.82, 97 cm = 0.57, 137 cm = 0.46) and caudal intraparietal (CIP) area (blue; proportions: 37 cm = 0.70, 57 cm = 0.87, 97 cm = 0.65, 137 cm = 0.55). (**F**) Proportion of neurons with significant orientation tuning at each possible number of distances for V3A (proportions: #0 = 0.11, #1 = 0.17, #2 = 0.22, #3 = 0.20, #4 = 0.30) and CIP (proportions: #0 = 0.06, #1 = 0.12, #2 = 0.23, #3 = 0.18, #4 = 0.41). (**G**) Comparison of surface orientation discrimination index (SODI) values at each distance for V3A (orange) and CIP (blue). Data points and error bars are mean and SEM across neurons with significant orientation tuning, respectively. The asterisk indicates a significant difference between V3A and CIP SODI values at 57 cm only (ANOVA followed by Tukey's HSD test, $p<0.05$).

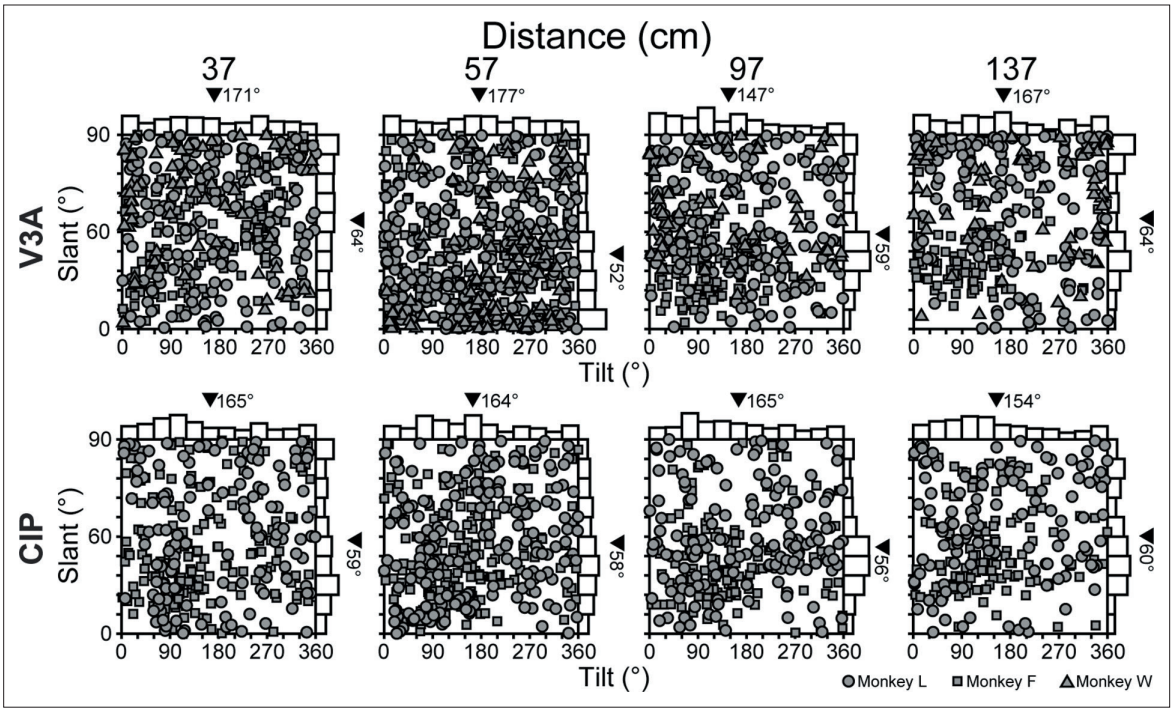

Figure 3—figure supplement 1. Distributions of 3D orientation preferences. Tilt and slant preferences in visual area V3A (V3A) (top row; 37 cm: N = 397 neurons; 57 cm: N = 570; 97 cm: N = 394; 137 cm: N = 317) and caudal intraparietal (CIP) area (bottom row; 37 cm: N = 304; 57 cm: N = 380; 97 cm: N = 283; 137 cm: N = 240) plotted using an equal area projection (***Rosenberg et al., 2013***). Marginal histograms show the distributions of tilt and slant. Black triangles mark mean values.

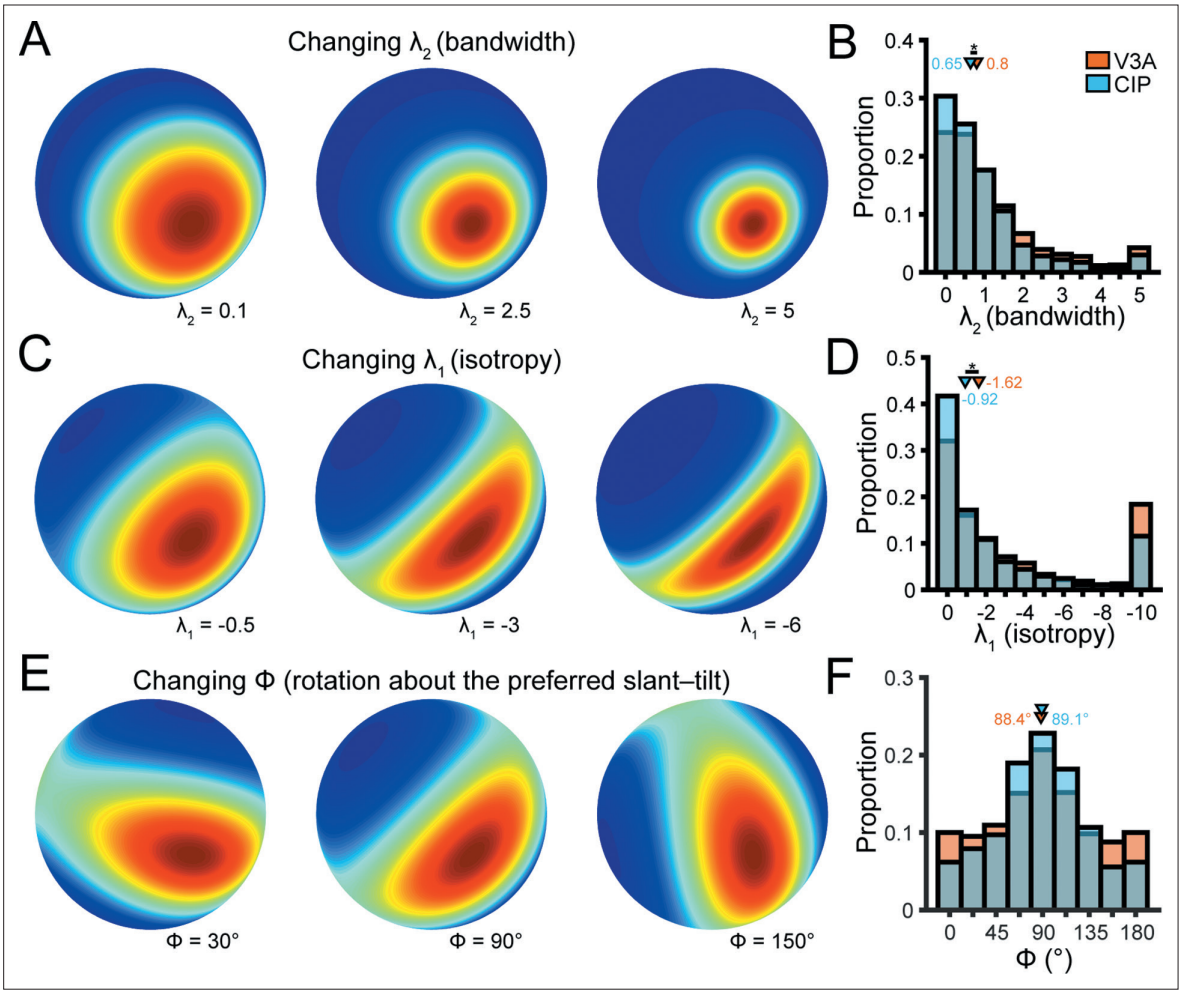

Figure 3—figure supplement 2. Cross-area comparison of 3D orientation tuning curve shape. Three Bingham function parameters set the bandwidth (λ_2), isotropy (λ_1), and axis about which tuning anisotropy occurred (Φ). (**A**) Bandwidth ($\lambda_2 \geq 0$). Larger values indicate narrower tuning. Fixed parameters in the schematic: $\lambda_1 = 0$, Φ = undefined since $\lambda_1 = 0$. (**B**) Distribution of λ_2 in visual area V3A (V3A) (orange bars) and caudal intraparietal (CIP) area (blue bars). (**C**) Isotropy ($\lambda_1 \leq 0$). More negative values indicate greater anisotropy. Fixed parameters in the schematic: $\lambda_2 = 0.7$ and $\Phi = 90°$. (**D**) Distributions of λ_1. (**E**) Axis about which tuning anisotropy occurred ($0° \leq \Phi < 180°$). Fixed parameters within the schematic: $\lambda_2 = 0.7$ and $\lambda_1 = -1.5$. (**F**) Distributions of Φ. Bars at 0° and 180° are identical. Distributions in (**C**, **E**, **G**) include all distances (V3A: N = 1,799; CIP: N = 1,276) and triangles mark median values. Asterisks in (**B**, **D**) mark significant cross-area differences (linear mixed-effects model with area and absolute distance from fixation as fixed effects and neuron as a random effect, $p<0.05$ for main effect of area).

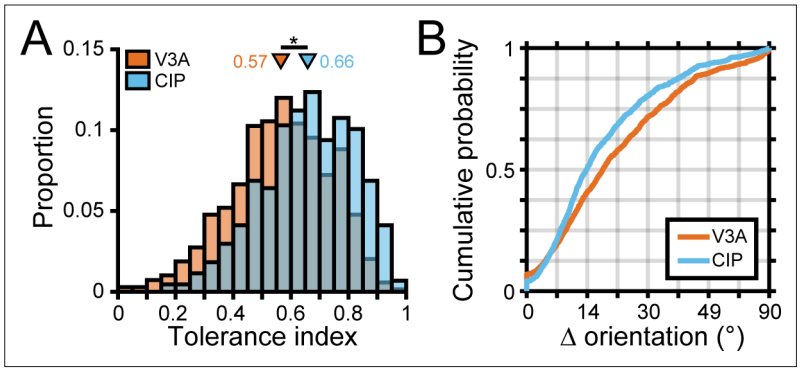

Figure 4. Robust 3D pose tuning was less prevalent in visual area V3A (V3A) than the caudal intraparietal (CIP) area. (**A**) Distribution of tolerance values in V3A (orange; N = 692) and CIP (blue; N = 437). Triangles mark mean tolerance values, and the asterisk indicates a statistically significant difference (two-sample *t*-test, $p<0.05$). (**B**) Cumulative density functions over the angular deviations between the orientation preference at each distance and the principal orientation for each neuron.

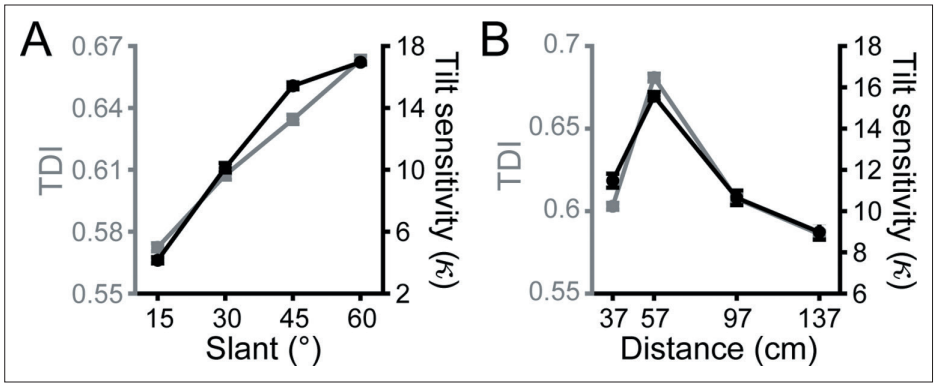

Figure 5. Neuronal correlates of tilt sensitivity. (**A**) Mean visual area V3A (V3A) tilt discrimination index (TDI) (gray) and behavioral tilt sensitivity (black) increased with slant. TDI values (and behavioral sensitivities) were averaged across neurons (or monkeys) and distances. (**B**) Mean V3A TDI and behavioral tilt sensitivity had an inverted U-shape relationship with distance. TDI values (behavioral sensitivities) were averaged across neurons (monkeys) and slants. Error bars are SEM.

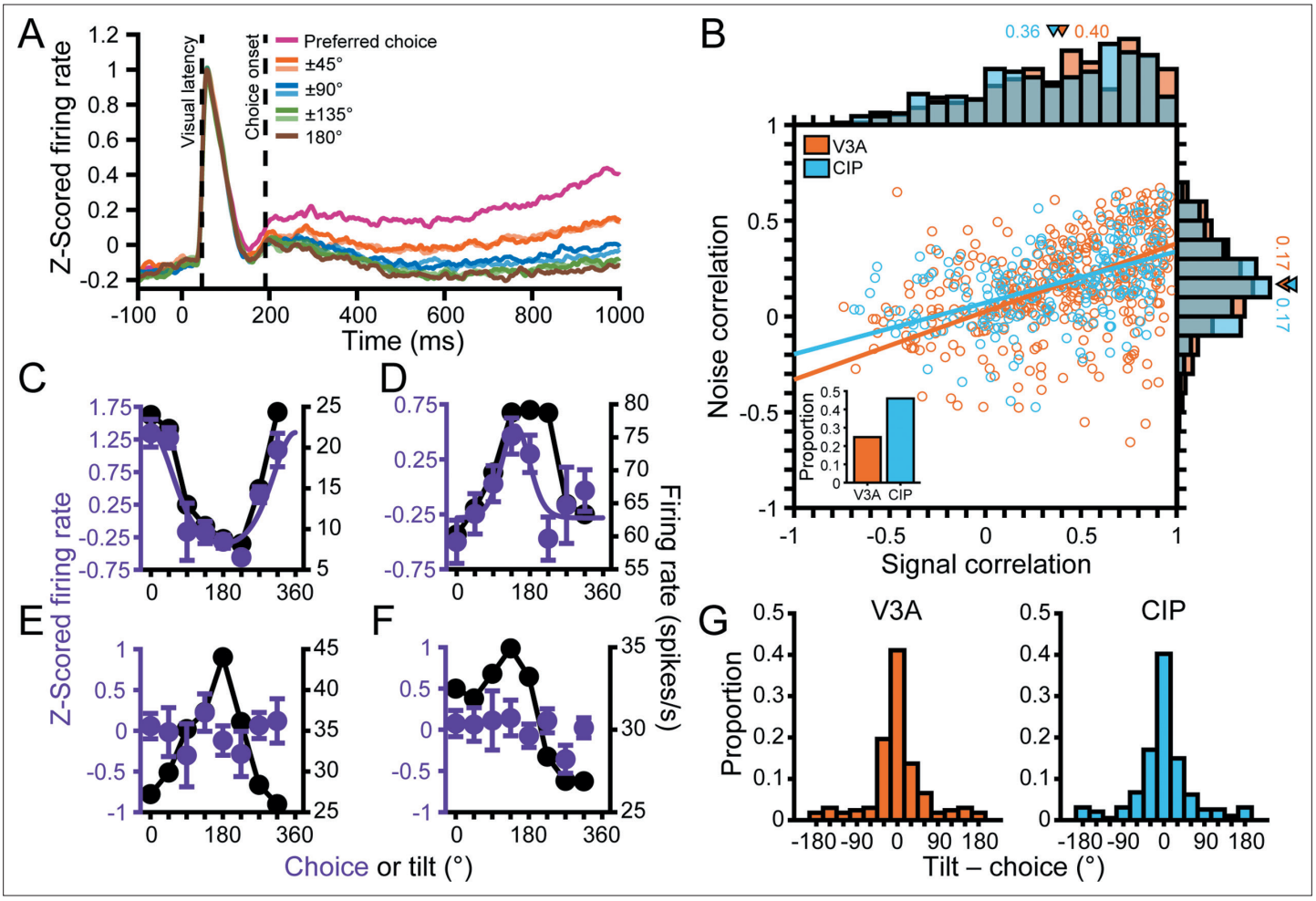

Figure 6. Choice tuning in visual area V3A (V3A) and its relationship to tilt tuning. (**A**) Population time courses for each choice option relative to the preferred choice. Curves show z-scored responses averaged over neurons. Stimulus onset = 0 ms. Vertical dashed lines mark the median visual response latency (46 ms) and the onset of choice-related activity (191 ms). (**B**) Comparison of noise and signal correlations in V3A (orange; N = 404 pairs) and the caudal intraparietal (CIP) area (blue; N = 244 pairs). Solid lines show type II linear regression fits. Marginal histograms show the distributions of noise (right) and signal (top) correlations. Triangles mark mean values. Inset shows proportion of neurons with choice-related activity in V3A (25%) and CIP (46%). (**C–F**) Choice tuning curves (left axis, purple) and tilt tuning curves marginalized over slant and distance (right axis, black) for the four example V3A neurons from ***Figure 3***. Data points show mean firing rate, and error bars are SEM. Solid purple curves are von Mises fits for neurons with significant choice tuning (ANOVA, $p<0.05$). Black lines are linear interpolations. (**G**) Comparison of preferred surface tilt and choice preferences in V3A (left, N = 168) and CIP (right, N = 194). The peaks near 0° indicate that the preferences generally aligned. Bars at ±180° are identical.

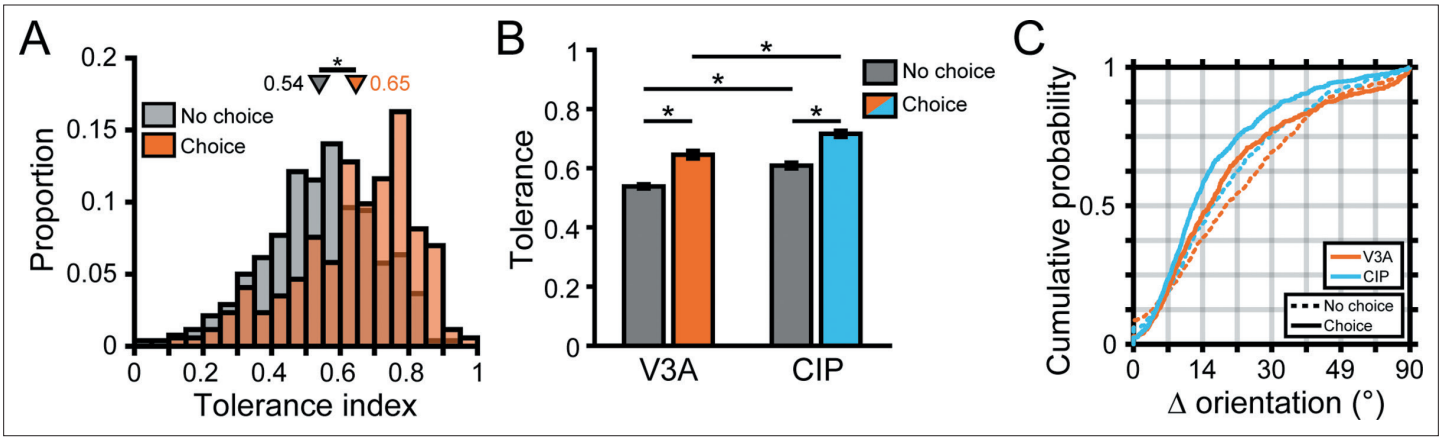

Figure 7. Robust 3D pose tuning was associated with choice-related activity. (**A**) Distribution of tolerance values for visual area V3A (V3A) neurons with (orange bars, N = 172) and without (gray bars, N = 520) choice-related activity. Triangles mark mean tolerances. (**B**) Cross-area comparison of tolerance values for neurons with (colored bars) and without (gray bars) choice-related activity. The V3A data in (**A**) is reproduced in (**B**) for comparison with the caudal intraparietal (CIP) area. Bar height indicates mean tolerance, and error bars are SEM. Horizontal lines and asterisks indicate significant differences in (**A, B**) (ANOVA followed by Tukey's HSD test, $p<0.05$). (**C**) Cumulative density functions over the angular deviations between the orientation preference at each distance and the principal orientation for neurons with (solid lines) and without (dashed lines) choice-related activity.

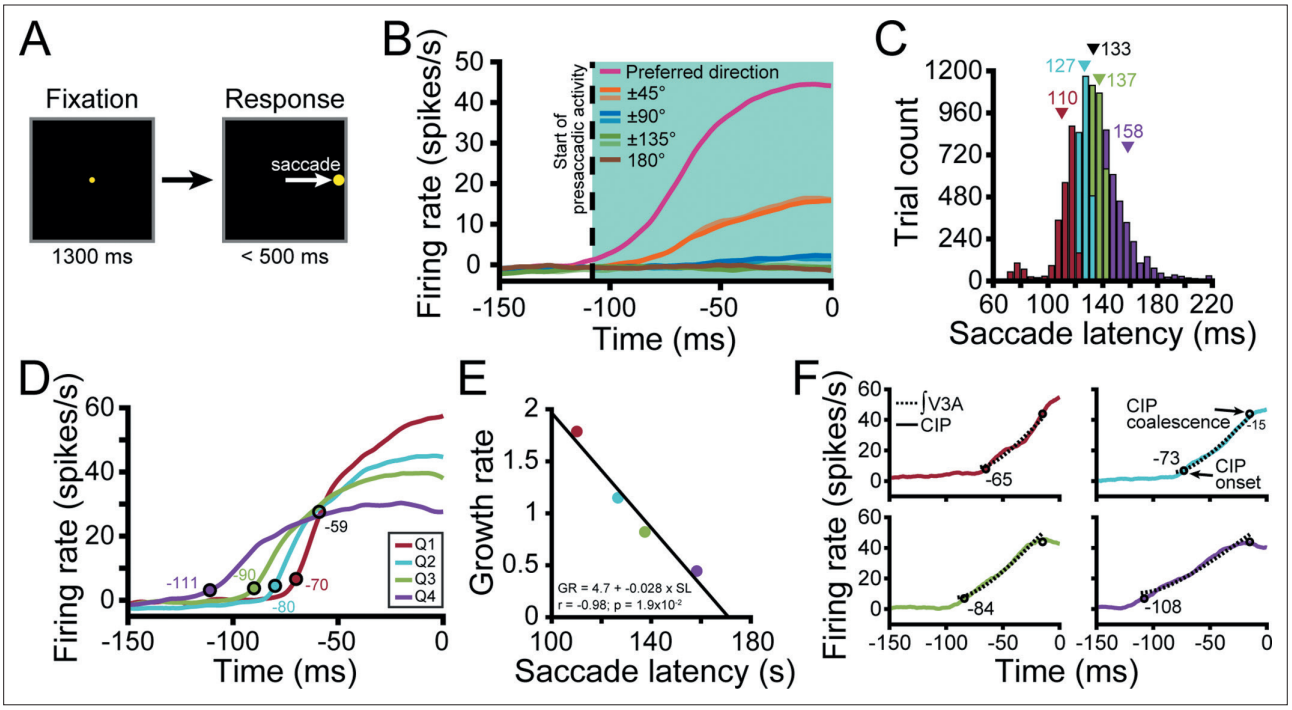

Figure 8. Saccade-related activity in visual area V3A (V3A). (**A**) Visually guided (pop-up) saccade task. A target was fixated for 1.3 s (matching the tilt discrimination task duration; left) after which it disappeared and a single saccade target appeared at one of eight locations (matching the choice targets in the tilt discrimination task; right). A saccade was then made to the target. (**B**) Population time courses for each saccade direction relative to the preferred direction. Curves show responses averaged over neurons. Saccade initiation = 0 ms. Vertical dashed line marks the start of saccade-related activity (–108 ms). (**C**) Histogram of saccade latencies divided into quartiles (Q). Triangles mark mean values (black for the full distribution). (**D**) Time courses of saccade-related activity conditioned on the saccade latency quartile. Colored circles mark the start of V3A activity for each quartile (ANOVA, $p<0.05$). Open black circle marks the point at which the V3A curves approximately coalesced. (**E**) Inverse linear relationship between the growth rate (GR) of saccade-related activity and mean saccade latency (SL) for each quartile. (**F**) The temporally integrated V3A time courses for each quartile (dashed curves) were well-aligned to the observed caudal intraparietal (CIP) area time courses (solid curves). Circles mark the start of CIP activity for each quartile and the point at which the curves approximately coalesced.

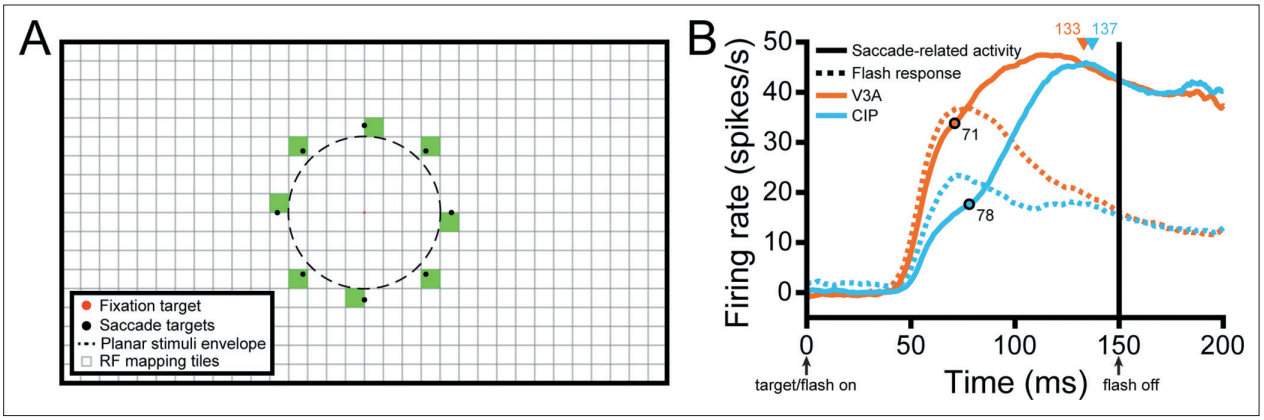

Figure 8—figure supplement 1. Comparison of saccade-related activity and responses to visual flashes without eye movements. (**A**) Screen schematic. Filled red and black circles show the fixation and choice/saccade targets, respectively. Dashed black circle shows the envelope of the planar stimuli. Squares show the tessellation for receptive field (RF) mapping in caudal intraparietal (CIP) area. Filled green squares are locations included in the analysis shown in (**B**). In visual area V3A (V3A), the mapped area was matched to the RFs (not shown). All elements are drawn to scale. (**B**) The saccade-related activity and responses to visual flashes had distinct time courses. The curves are population-averaged responses to the preferred saccade directions (solid curves) and visual flashes at nearby RF mapping tiles (bright flashes only; dashed curves). For V3A, 390/415 neurons with saccade-related activity were included. The others were removed because the preferred saccade target was outside of where the visual RF was mapped. For CIP, all 274 neurons with saccade-related activity were included. Visual flashes were 150 ms in duration. Saccade targets were present until the eyes entered the saccade target window (triangles mark median saccade onset times). Despite the visual flashes being of higher contrast (Weber contrast = 2.2) and larger (1.9° × 1.9° in V3A, 3.9° × 3.9° in CIP) than the saccade targets (Weber contrast = 1.0; 0.7° diameter), the flash responses were weaker and more transient than the saccade-related activity. The saccade-related activity also had conspicuous inflection points at 71 ms in V3A and 78 ms in CIP (marked by open black circles; calculated by finding when the second derivative equaled zero), which speculatively reflect the addition of presaccadic activity to an otherwise visual transient.

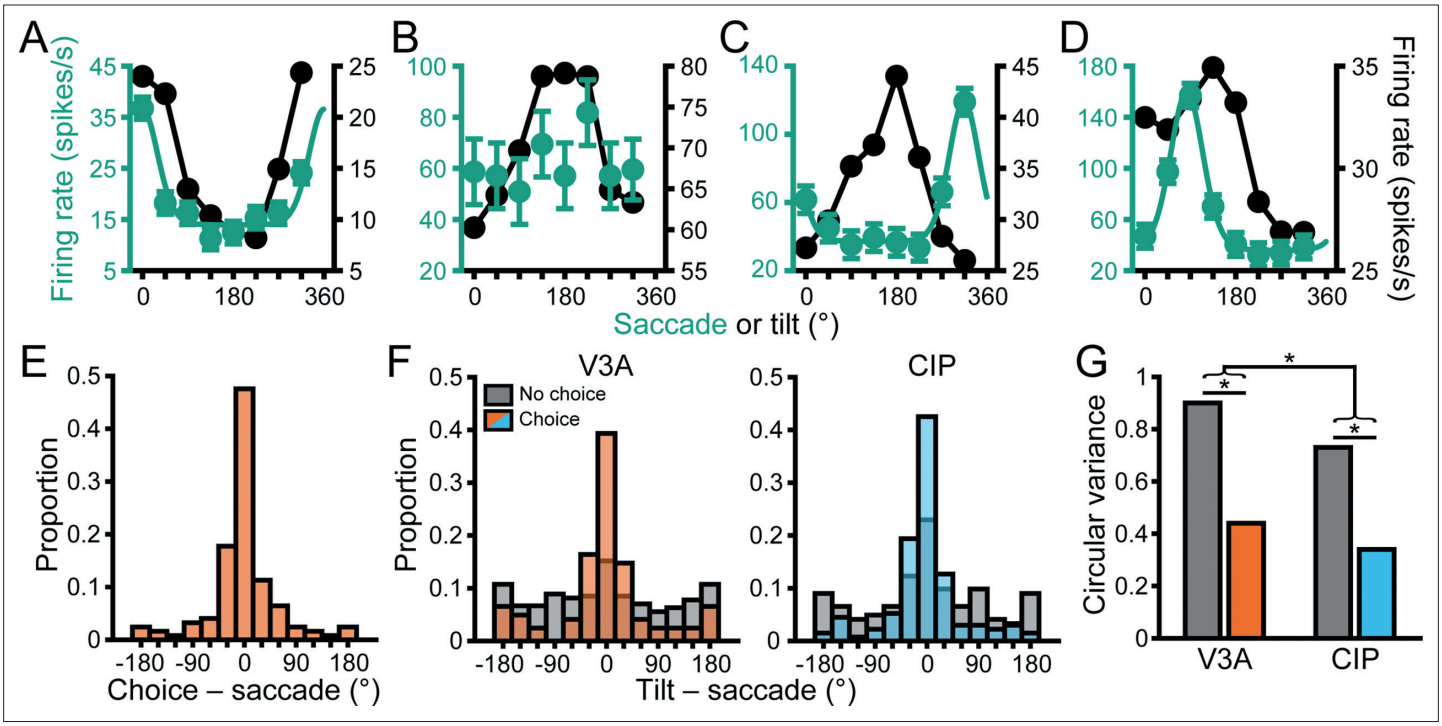

Figure 9. Sensorimotor associations were moderated by choice-related activity. (**A–D**) Saccade direction tuning curves (left axis, green) and tilt tuning curves marginalized over slant and distance (right axis, black) for the four example visual area V3A (V3A) neurons from ***Figures 3 and 6***. Data points are mean firing rates and error bars are SEM across trials. Solid green curves are von Mises fits for neurons with significant saccade direction tuning (ANOVA, $p<0.05$). Black lines are linear interpolations. (**E**) Differences between choice and saccade direction preferences in V3A (N = 124). (**F**) Differences between principal surface tilts and saccade direction preferences for neurons with (colored bars) and without (gray bars) choice-related activity in V3A (left) and caudal intraparietal (CIP) area (right). Bars at ±180° are identical in (**E, F**). (**G**) Comparison of circular variances for the distributions in (**F**). Horizontal lines and asterisks indicate significant differences (two-sample concentration difference test, $p<0.05$).

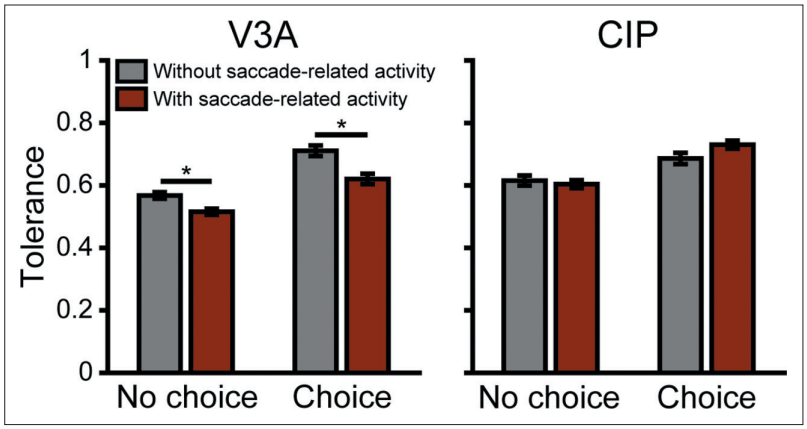

Figure 9—figure supplement 1. Saccade-related activity was associated with less robust 3D tuning in visual area V3A (V3A), but not caudal intraparietal (CIP) area. Tolerance values were compared for neurons with and without saccade-related activity, condition on the presence of choice-related activity in V3A and CIP. Four neuronal subpopulations were defined: those with (1) choice- and saccade-related activity (C+S + , V3A: N = 124; CIP: N = 137), (2) choice- but not saccade-related activity (C+S-, V3A: N = 48; CIP: N = 64), (3) no choice- but saccade-related activity (C-S+, V3A: N = 291; CIP: N = 137), and (4) neither choice- nor saccade-related activity (C-S-, V3A: N = 229; CIP: N = 99). First, we compared neurons with choice-related activity (C+S + and C+S-). Tolerance values were significantly lower for C+S+ than C+S- neurons in V3A ($p=6.9 \times 10^{-3}$) but not CIP (p=0.23). Second, we compared neurons without choice-related activity (C-S+ and C-S-). Tolerance values were significantly lower for C-S+ than C-S- neurons in V3A ($p=1.9 \times 10^{-3}$) but not CIP (p=0.94). Thus, saccade-related activity was associated with less robust 3D tuning in V3A. There was no significant relationship between saccade-related activity and the robustness of 3D tuning in CIP. Horizontal lines and asterisks indicate significant differences (ANOVA followed by Tukey's HSD test, $p<0.05$).